Climate Dynamics
https://doi.org/10.1007/s00382-023-06938-w

Aleutian low/PDO forces a decadal subsurface spiciness propagating mode in the North Pacific

Sieu-Cuong San[1] · **Yu-heng Tseng**[1,2]

Received: 29 May 2023 / Accepted: 20 August 2023

Abstract
Analysis of observational data reveals the existence of a decadal subsurface spiciness mode that involves ocean–atmosphere coupling in the North Pacific. Specifically, the Aleutian Low, the dominant atmospheric forcing of the Pacific Decadal Oscillation (PDO), drives a dipole pattern of positive and negative spiciness anomalies in the eastern midlatitude and subtropics, respectively. These anomalies then propagate equatorward along a deflected route defined by the mean acceleration potential. The positive spiciness anomaly can be observed at 14° N after 7 years of propagation while the downstream negative anomaly can be tracked to 10° N after 3 years from its appearance. In addition, a negative spiciness anomaly appears in the midlatitude, followed by the formation of the positive spiciness anomaly 2 years later. It follows a similar pathway toward the tropics. Further analysis demonstrates a strong connection between equatorial sea surface temperature variability and extratropical spiciness anomalies. These processes, in turn, potentially lead to a decadal climate oscillation in the North Pacific involving extratropical-tropical interaction. The dominant physical processes responsible for subsurface spiciness variability differ significantly between the eastern midlatitude and subtropical North Pacific. In the midlatitude, isopycnal spiciness variability exhibits similar characteristics to temperature variations at around 50–120 m depth, mainly generated through subduction and reemergence processes. Conversely, interior subtropical spiciness variability follows the evolution of salinity anomalies at around 120–250 m and is mainly formed via subduction and spice injection. Furthermore, anomalous advection across mean spiciness gradients strengthens subsurface signals from the midlatitude to the subtropics.

Keywords Aleutian Low/PDO · Subsurface spiciness mode · Subduction · Spice injection · Anomalous advection across mean spiciness gradients

1 Introduction

The low-frequency dynamics of subsurface temperature/salinity anomalies in the eastern Pacific Ocean have long been an active theme of research due to their important role in connecting extratropics with the tropics (Gu and Philander 1997; Schneider 2000, 2004). Based on Gu and Philander (1997)'s hypothesis, Liu (2012) suggested the following extratropical-tropical coupling: after a positive temperature anomaly is formed in the subtropical North Pacific, it is then advected adiabatically by the mean current westward and equatorward along isopycnal surfaces toward the tropical region (Sasaki et al. 2010; Kolodziejczyk and Gaillard 2012). Along the equator, the anomaly flows eastward by the Equatorial Undercurrent (EUC), upwells, and warms the surface in the central-eastern equatorial Pacific. The surface warming also concurrently relaxes the local easterlies. Therefore, this warming is further enhanced via the positive Bjerknes feedback. Subsequently, equatorial warming forces the excitation of a wave train or wave signal that extends into the extratropical North Pacific (Alexander 1990, 1992). This atmospheric perturbation modulates the strength of the Aleutian Low, zonal wind anomalies, and hence turbulent heat flux in the midlatitude. Eventually, a negative subsurface temperature anomaly is generated and then propagates along a similar path of the positive anomaly toward the equator. This could form decadal climate variability in the North Pacific with the time scale determined by the equatorward

✉ Yu-heng Tseng
tsengyh@ntu.edu.tw

[1] Institute of Oceanography, National Taiwan University, Taipei, Taiwan

[2] Ocean Center, National Taiwan University, Taipei, Taiwan

Published online: 02 September 2023

ventilation of the anomalous signals (Gu and Philander 1997).

These early studies suggested the key role of subsurface temperature/salinity anomalies in the tropical-extratropical interaction for Pacific decadal climate variability. The generation of subsurface temperature/salinity anomalies can be classified into two distinct mechanisms: subduction and injection. Subduction occurs when an isopycnal (a surface of constant density) is exposed to the surface, allowing sea surface signals to follow the outcrop line toward the interior ocean (Nonaka and Sasaki 2007; Kolodziejczyk and Gaillard 2012). Therefore, the meridional displacement of the outcrop line which is governed by the compensated contribution of sea surface temperature (SST) and sea surface salinity (SSS) anomalies determines the positive or negative sign of the anomalies on the isopycnal surface (Nonaka and Sasaki 2007). This mechanism generates anomalies locally, i.e., just below the position of the outcrop line. The injection mechanism (spice injection), on the other hand, generates subsurface anomalies further equatorward away from the isopycnal outcrop position and is responsible for the positive anomalies (Yeager and Large 2004; Luo et al. 2005; Kolodziejczyk and Gaillard 2012; Wang and Luo 2020). The injection occurs when the examined isopycnal does not expose to the surface, but the large unstable vertical salinity gradient in conjunction with weak stratification in winter favors convective mixing at the base of the mixed layer (Yeager and Large 2004). As a result, the surface saline water is injected into the ocean interior, creating a density-compensating layer of temperature and salinity anomalies, termed spiciness anomalies, at the base of the mixed layer (Yeager and Large 2004; Wang and Luo 2020). Furthermore, subsurface anomaly generation involving atmospheric stochastic forcing is also proposed. In particular, the ocean filters the overlying atmospheric noise (Hasselmann 1976) resulting in a large-scale first baroclinic mode pressure response. The anomalous geostrophic advection then crosses the mean spiciness gradients which in turn generate low-frequency subsurface spiciness variability (Kilpatrick et al. 2011). Isopycnal spiciness anomaly formation via this mechanism has also been shown to dominate in model simulations, leading to a decadal spiciness mode in the tropical North Pacific (Schneider 2000).

The spiciness variable, which is often represented as temperature or salinity on a certain isopycnal surface (Kolodziejczyk and Gaillard 2012; Li et al. 2012; Zeller et al. 2021), has been increasingly employed in recent literature to investigate low-frequency ocean climate variability. Initially, spiciness (or potential spicity) was constructed as a state variable to characterize the remaining information of thermodynamics not included by potential density. Therefore, isolines of spiciness were required to be orthogonal to potential density in the T-S diagram (Stommel 1962; Veronis 1972; Munk 1981; Müller and Willebrand 1986; Huang 2011; Huang et al. 2018). Spiciness defined in this way was assumed to be dynamically passive, accurately measuring mixing along isopycnal surfaces (Veronis 1972). However, later studies identified that such an orthogonal constraint is ambiguous because the scaling in the axes of the T-S diagram can vary in tandem with the thermal expansion and haline contraction coefficients (Jackett and Mcdougall 1985; Flament 2002; McDougall and Krzysik 2015). In addition, the passive behavior of spiciness lies in its variations along isopycnal surfaces but not as an inherited property of any thermodynamic variable (McDougall and Krzysik 2015; McDougall et al. 2021). McDougall and Krzysik (2015) sacrificed the orthogonal enforcement but strictly required the variation of spiciness along isopycnal surfaces to be proportional to the isopycnal water-mass variations, expressed in density units. The solid theory for the construction of spiciness remains a matter of ongoing debate, and it is largely evolving along two main streams: orthogonality (Huang et al. 2021) and nonorthogonality (McDougall et al. 2021) with potential density in the T-S diagram. Recently, Tailleux (2021) suggested that before the construction of spiciness, a neutral density variable (Tailleux 2016) that is materially conserved should be well-defined first, and then any material density function can be used to construct spiciness quantified in terms of its anomaly along the neutral surfaces.

One appealing question is whether the advection of remotely generated spiciness anomalies by the mean current can effectively migrate to the equator and impact tropical climate variability. Modeling (Schneider et al. 1999b; Pierce et al. 2000; Schneider 2000; Giese et al. 2002; Fukumori et al. 2004; Yeager and Large 2004) and observational studies (Schneider et al. 1999a; Zhang and Liu 1999) have yielded ambiguous conclusions regarding the propagation of such signals from the extratropical subduction zone in both hemispheres. On the one hand, some studies have demonstrated that the magnitude of spiciness anomalies diminishes significantly during propagation (Liu and Shin 1999; Sasaki et al. 2010; Kolodziejczyk and Gaillard 2012) and likely cannot reach the western equatorial Pacific (Schneider et al. 1999a; Hazeleger et al. 2001). On the other hand, some studies have found that spiciness anomalies can spread to the equator via the interior pathway (Luo et al. 2005; Li et al. 2012) and/or the western boundary pathway (Yeager and Large 2004; Luo et al. 2005; Sasaki et al. 2010; Kolodziejczyk and Gaillard 2012) but with a much-reduced amplitude. Moreover, the relative contribution of mean advection of spiciness anomalies along the interior pathway versus the western boundary pathway at each hemisphere to the

low-frequency signal peak in the equator is subject to event dependence. Employing an ocean general circulation model combined with a Lagrangian particle simulation forced with surface climatological conditions, Zeller et al. (2021) demonstrated that a positive event peak in the subsurface equator is mainly contributed by Southern Hemisphere water traveling along the interior pathway while the other negative event peak is primarily caused by water traveling via the western boundary pathway in the Northern Hemisphere. These studies suggested that tropical ocean variability can be influenced by extratropical signals. Despite numerous efforts attempting to understand the role of extratropical signals on interannual to decadal tropical climate variability, a comprehensive understanding regarding the surface forcing of subsurface spiciness anomaly (SSA) as well as the dominant physical processes responsible for the formation of isopycnal spiciness anomalies in the North Pacific remains unclear.

In this study, we characterize a low-frequency subsurface spiciness propagating mode in the North Pacific and directly link it with the Aleutian Low/Pacific Decadal Oscillation (PDO) using two different observational datasets. The Aleutian Low is the dominant sea level pressure (SLP) pattern in the North Pacific primarily driven by internal atmospheric dynamics (Pierce 2001; Alexander et al. 2010) while the PDO (Mantua et al. 1997) can be regarded as the oceanic expression of high-frequency atmospheric variability (Newman et al. 2003; Newman et al. 2016; Schneider and Cornuelle 2005). To the best of our knowledge, this is the first study to establish a connection between SSAs and the Aleutian Low/PDO. Furthermore, we clarify the physical processes responsible for isopycnal spiciness variability in the midlatitude and subtropics, respectively. We find that the net surface heat flux (Qnet) and wind stress curl anomalies associated with the Aleutian Low/PDO create SSAs via subduction and spice injection mechanisms. In addition, changes in ocean circulation related to the interaction between the Aleutian Low and PDO contribute to the strengthening of subsurface spiciness signals through the anomalous advection across the mean spiciness gradient mechanism. This paper is organized as follows. Section 2 describes the data and the method utilized. Section 3 presents the main results of the study, followed by discussion and concluding remarks in Sects. 4 and 5, respectively.

2 Data and methodology

For the ocean subsurface temperature and salinity, we utilize the latest EN.4.2.2 in the 'EN' series of data sets from the Met Office Hadley Centre (Good et al. 2013), 1° horizontal grids over 42 non-uniform spaced depth levels spanning from 1900 to the present at monthly intervals. The dataset incorporates all available sources of oceanographic measurements, primarily from the World Ocean Database 2009 (WOD09). Four ensemble members are available in EN.4.2.2. EN.4.2.2.analyses.g10 (hereinafter referred to as EN422) is chosen for our analysis while the results extracted from the other three ensembles are qualitatively consistent and similar. In addition, the gridded Grid Point Value of the Monthly Objective Analysis (MOAA GPV) (Hosoda et al. 2008) is also used to compare the evolution of subsurface anomalies during 2001–2019. The MOAA GPV is constructed mainly from Argo floats in combination with buoy measurements and casts of research cruises. The horizontal resolution is 1° on standard pressure levels between 10 and 2000 dbar. For sea surface height (SSH) data, we use the Global Ocean Data Assimilation System (GODAS) with a resolution of 0.33° latitude by 1° longitude during 1980–2019 (Behringer et al. 1998; Behringer and Xue 2004). Furthermore, the SLP, SST, and 10-m wind data from the ERA5 (Hersbach et al. 2020) are used. To be consistent with atmospheric data, our analysis uses the period from 1979 to 2019 except for MOAA GPV which is analyzed from 2001 to 2019.

The temperature and salinity are first converted to conservative temperature and absolute salinity based on the TEOS-10 (McDougall and Barker 2011) before calculating spiciness following the method proposed by Jackett and Mcdougall (1985) and McDougall and Krzysik (2015):

$$\int_{\rho^{\Theta}} d\pi = 2 \int_{\rho^{\Theta}} \left. \frac{\partial \rho^{\Theta}}{\partial S_A} \right|_{\Theta, p_r} dS_A \tag{1}$$

$$\pi_0\left(S_A, \Theta\right) = \pi_u \sum_{j=0}^{6} \sum_{k=0}^{6} A_{jk} s^j y^k \tag{2}$$

where π is spiciness, Θ is conservative temperature, S_A is absolute salinity, ρ is potential density, p_r is reference pressure, π_0 is spiciness referenced to 0 dbar, $\pi_u = 1$ kg m^{-3}, A_{jk} is the coefficients of the polynomials for spiciness, s is the nondimensional salinity, and y is the nondimensional temperature (see McDougall and Krzysik (2015) for more details). The spiciness in the pressure coordinates is then transformed to sigma coordinates by linear interpolation on the isopycnals $\sigma_\theta = 25$–26 with $\Delta\sigma_\theta = 0.01$ kgm^{-3}. The chosen isopycnal level is within the main thermocline (Fig. S1). It can capture a larger portion of the spiciness signal formation compared to that typically defined using 25–25.5 σ_θ (not shown), and thus more appropriately tracking water mass from the source generation region to the tropics. To remove the impacts of the annual cycle, the interpolated data are filtered with a 13-month running mean. We also analyze

the spiciness based on the definition of Huang et al. (2018). The results are qualitatively similar despite some small differences in the magnitude of the anomalies.

To account for the pathway connecting extratropics with the tropics, we calculate the mean acceleration potential, referenced to 2000 dbar (McDougall and Klocker 2010). It is then interpolated to sigma coordinates and low-pass filtered with a 13-month running mean. Since the interior and western boundary pathways are not explicitly separated here, we define the North Pacific Pathway (hereinafter referred to as NPP) as the passage between the acceleration potential contours of 19.7 and 21 m^2s^{-2} which covers a large portion of the extratropical-tropical exchange window to describe the propagation features.

The temporal and spatial characteristics of low-frequency spiciness variability are investigated using a complex empirical orthogonal functions (CEOF) analysis (Barnett 1983; Horel 1984) performed in the North Pacific (0–60° N, 120° E–80° W). The advantage of CEOF over traditional empirical orthogonal function (EOF) analysis lies in its ability to extract propagating properties in the data by providing not only the amplitude but also the potential phase change. Given the propagating nature of isopycnal spiciness anomalies, this method can reveal important propagation properties related to the fate of spiciness variability (see Text S1 for more details). The statistical significance of the correlations and regressions is assessed utilizing a two-tailed Student's t-test. All statistical analyses are conducted at a 95% confidence level unless otherwise specified. The estimation of the number of effective degrees of freedom follows the approach proposed by Davis (1977).

3 Results

3.1 Characteristics of low-frequency spiciness variability

The CEOF analysis of spiciness anomalies averaged between 25 and 26σ_θ has identified the dominant mode of low-frequency variability in the North Pacific. This mode accounts for approximately 28% and 51% of the total spiciness variance in the EN422 and MOAA GPV datasets, respectively (Fig. 1). It is significantly distinguished from the rest modes and exhibits the most prominent propagating feature (Figs. 1c, d and 2). Therefore, we focus entirely on the first CEOF mode (CEOF1) in this study. The spatial amplitude of CEOF1 is similar between the EN422 and MOAA GPV although the latter shows a weaker magnitude in the eastern midlatitude (Fig. 1a, b). These differences are attributed to the different periods covered by each dataset. In general, CEOF1 exhibits maximum variability equatorward from the outcropping area, centered at 38° N, 140° W. The associated magnitude reaches 0.12 kg m^{-3} in the center of action but decreases considerably downstream along the NPP as indicated by the acceleration potential contours of 19.7 and 21 m^2s^{-2}. This area of maximum spiciness variability is consistent with that identified by Li et al. (2012) based on potential temperature averaged between 25 and 25.5σ_θ from the MOAA GPV dataset. While CEOF1 of the present study possesses only one center of maximum variability in the extratropics, Li et al. (2012) showed another secondary variability in the eastern subtropical region around 20°

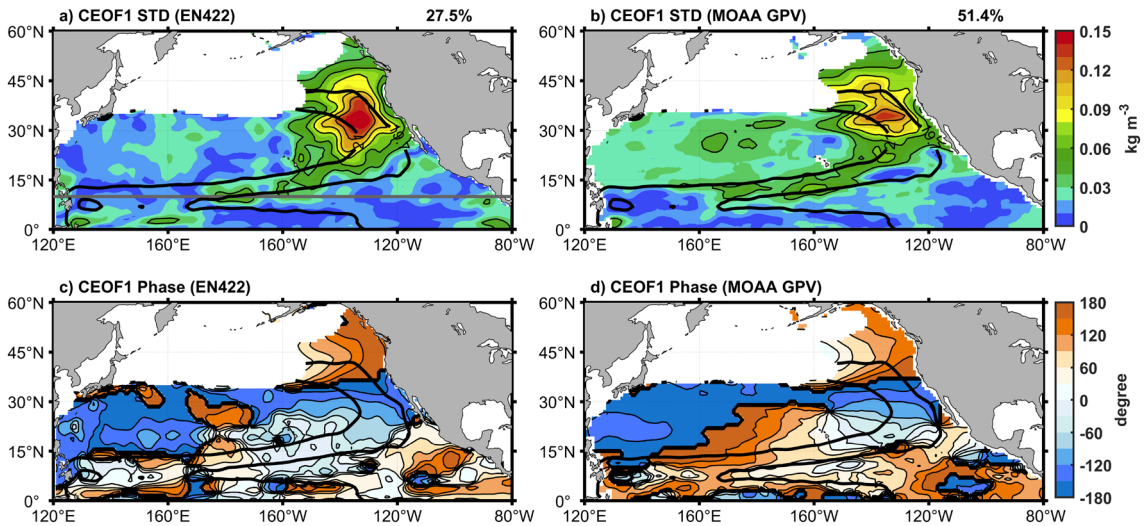

Fig. 1 **a** Standard deviation of low-frequency spiciness variability (kg m^{-3}) averaged between 25 and 26σ_θ in the North Pacific associated with CEOF1 for EN422. **b** same as **a** but for MOAA GPV. **c** and **d** are the corresponding spatial phase (in degree) of the leading mode derived from EN422 and MOAA GPV, respectively. The thick black lines denote the mean acceleration potential contours of 19.7 and 21.0 m^2s^{-2} (NPP). The gray line in **a** indicates the latitude of 10° N

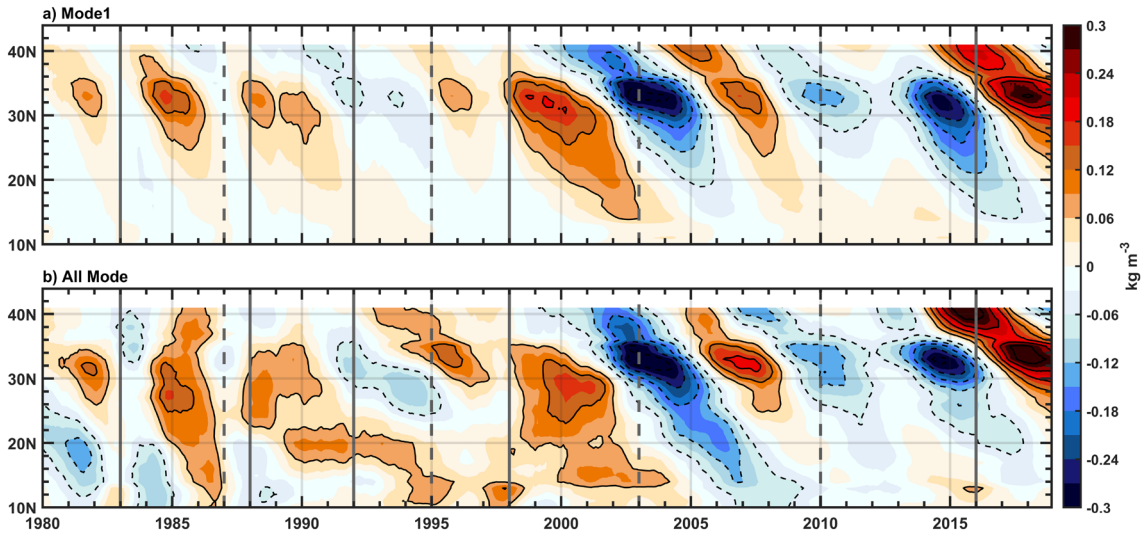

Fig. 2 Latitude-time diagram of reconstructed spiciness anomalies (kg m^{-3}) using the **a** first and **b** all CEOF modes averaged along the NPP based on EN422. The vertical solid (dashed) gray lines represent strong and very strong (moderate) El Niño events that peak in January based on the Niño3.4 SST index (5° S–5° N, 170°–120° W)

N east of 130° W. Compared to the CEOF1 of interannual salinity anomalies evaluated on the $\sigma_\theta = 25.5$ surface by Kolodziejczyk and Gaillard (2012), the spiciness signal in the present study is much more coherent and stronger, and the center of action expands further northward to about 50° N (Fig. 1). These differences may ascribe to the isopycnal levels considered, which are deeper than the $\sigma_\theta = 25$–25.5 isopycnal levels used in the two previous studies.

A propagating signal is evident from the increasing spatial phase of CEOF1 along the NPP (Fig. 1c, d). This propagating feature is further demonstrated by reconstructing CEOF1 from -180° to 180° at every 45° phase interval (Fig. S2). The abrupt zonal change of phase around 38° N coincides with the large variance of the first mode. At lower latitudes, the phase structure is strongly modulated by the turn to the eastern edge of the pathway where the potential vorticity barrier (Lu and McCreary 1995) hinders the direct equatorward transport from the extratropics to the tropics. Though the spatial phase along the NPP is qualitatively similar between the two datasets poleward of 20° N, significant differences can be observed downstream. While the MOAA GPV shows a smoother phase transition, the EN422 experiences a significant phase change which is probably due to the decadal changes in the propagating characteristics. These will be further shown next.

The propagating characteristics of the first and all CEOF modes are assessed by reconstructing the spiciness anomalies on the Hovmöller diagram along the NPP (Fig. 2). During 1980–2018, there are episodes of positive and negative spiciness anomalies that occur in the extratropical North Pacific (Fig. 2a). The alternating anomalies (two negative and one positive) during 2003–2011 have been previously reported (Sasaki et al. 2010; Kolodziejczyk and Gaillard 2012; Li et al. 2012) (Fig. 2). In addition, two major spiciness events of opposite signs emerge from 2012 onwards: one negative anomaly appeared in 2012–2013, and the other positive anomaly originated in 2014–2015. Our results suggest that considering deeper isopycnal levels can characterize the spiciness occurrence (variability) from the high latitude region at least 1–2 years in advance compared to previous studies.

The reconstructed spiciness anomalies based on CEOF1 show a clear equatorward propagation with the strongest variability observed poleward of 24° N, consistent with the spatial distribution of amplitude (Figs. 1 and 2a). A positive spiciness anomaly centering at 35° N, 130° W propagates westward and equatorward along the NPP (– 180°, Fig. S2), corresponding with the increasing phase (Figs. S2 and 3). The magnitude is then gradually reduced (– 45° to 180°, Figs. 2 and S2). In addition, a negative spiciness anomaly formed in the midlatitude North Pacific centering at 40° N, 150° W subsequently follows the same pathway as the positive one takes to reach the tropics (–135°, Figs. 2 and S2). As a result, the equatorward propagation of prominent spiciness anomalies from 40° to 10° N lasts for about 7 years (Figs. 2a and S2) which is consistent with the temporal phase change (Fig. 3). This time scale is in good agreement with the estimated 7–8 years for the extratropical origin of subsurface signals to reach the tropics (Schneider et al. 1999a; Kolodziejczyk and Gaillard 2012). Our study also reveals that the propagating signals along the NPP can reach 10° N, especially after 1998/1999 (Fig. 2). The more equatorward arrival of spiciness anomalies after 1998/1999 on the one hand may result from the

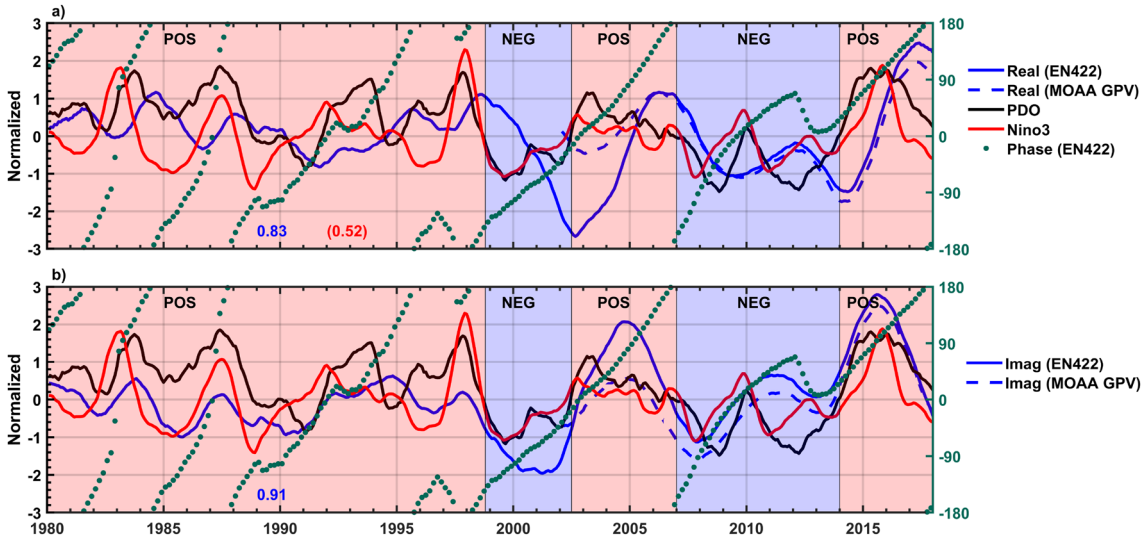

Fig. 3 Normalized time series of **a** real and **b** imaginary expansion coefficients of CEOF1. The associated temporal phase (in degree) of the CEOF1 is shown as green dots. The black and red lines are the PDO index from the NOAA Physical Sciences Laboratory (https://psl.noaa.gov/pdo/) and Niño3 (5° S–5° N, 150°-90° W) index obtained from the NOAA Climate Prediction Center (http://www.cpc.noaa.gov/products/analysis_monitoring/ensostuff/ensoyears.shtml), respectively. The blue numbers in **a** and **b** are the simultaneous correlation between PC1 (real and imaginary parts, respectively) of spiciness anomalies derived from MOAA GPV and EN422 during the same period (2002–2018). The red number in **a** is the simultaneous correlation between the PDO and the Niño3. POS and NEG correspond to PDO's positive and negative phases

decadal change of the intertropical convergence zone. In particular, the width of the intertropical convergence zone has narrowed in recent decades as a response to climate change (Byrne et al. 2018) and thus weakening the potential vorticity barrier in the lower layer (Lu and McCreary 1995) to facilitate the equatorward propagation of extratropical signals. Here, we note that the poor-quality data during the pre-Argo period (before 2001) might be another possibility contributing to the discrepant signal before and after 1998/1999. However, this was not easy to confirm in the current study.

Nevertheless, there is a substantial difference between the spiciness signals before and after 1998/1999 (Fig. 2), which corresponds to the period of the North Pacific SST and atmospheric conditions abrupt change, known as the climate regime shift occurring after the winter of 1998/1999 (Lyon et al. 2014). This regime shift resulted in shorter persistence of the PDO cold/warm phases since 1998/1999 compared to the prolonged warm condition before the shift (Fig. 3). For comparison, the temporal evolution of the first principal component (PC1) of spiciness anomalies is also shown in Fig. 3. While the imaginary component almost varies in tandem with the PDO index, the real part of spiciness anomalies lags the PDO by 18–24 months with a strong correlation (Fig. 4a), suggesting a relevance between the two leading modes of surface and subsurface oceanic variability in the North Pacific (Fig. 3). This will be elaborated more in the next section.

3.2 Forcing mechanism

Motivated by the linkage between PDO and the PC1 (real) of spiciness anomalies, we further investigate the role of PDO in forcing subsurface variability in the extratropical North Pacific. All subsequent analyses are based on the long-term EN422 dataset unless otherwise noted (conclusions are not sensitive to the specific dataset employed). Defined as the leading EOF of monthly SST anomalies (SSTA) poleward of 20° N (Mantua et al. 1997), the spatial pattern of the positive PDO phase is characterized by a positive anomaly extending from the high latitude toward the equator along the west coast of North America, combined with a negative anomaly in the western-central Pacific (Fig. S3a). As the SLP and 10-m wind vector anomalies are regressed onto the PDO index, an intense cyclonic circulation corresponding with the strengthening of the Aleutian Low can be found in the North Pacific (Fig. S3b). In addition, the interannual variability of the Aleutian Low (defined as the principal component of the leading EOF of interannual SLP anomalies between 20°–60° N, 120° E–80° W) shows a strong correlation with PDO, reaching a simultaneous correlation of 0.63 and as high as 0.68 when the Aleutian Low leads the PDO for three months (Fig. S3c). This result is consistent with previous studies (Schneider and Cornuelle 2005; Newman et al. 2016).

Comparing the spatial structure of CEOF1 (Fig. 1) with the PDO pattern (Fig. S3a) and its associated atmospheric forcing (Fig. S3b), we find that the region of maximum

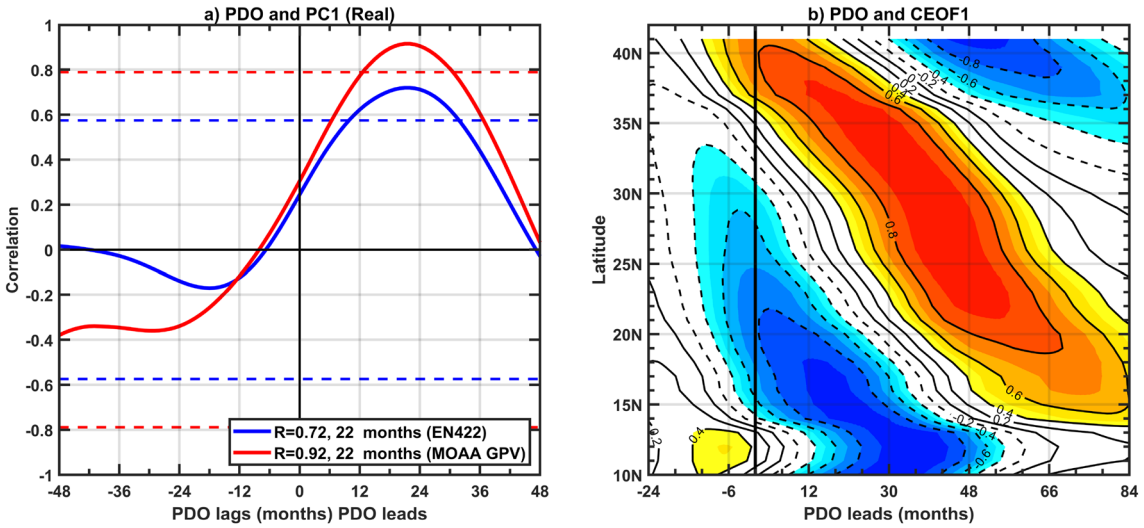

Fig. 4 **a** Lead-lag correlation coefficients between the PC1 of spiciness anomalies and the PDO index. Horizontal dashed lines indicate the 95% confidence level. **b** Lead-lag correlation coefficients between the PDO index and reconstructed spiciness anomalies using CEOF1 averaged along the NPP. The thick black line in (**b**) indicates lag 0. Positive lags indicate PDO leads the spiciness anomalies

spiciness variability aligns with the south-eastward extension of the positive temperature anomaly below the center of the Aleutian Low. The pattern of SSTA regressed onto the PC1 of spiciness anomalies (shading in Fig. S4) closely resembles the positive phase of the PDO. The forcing of PDO is further confirmed by the lead-lag correlation between the PDO index and the PC1 (real) of spiciness anomalies (Fig. 4a). As expected, the highest correlation occurs when the PDO leads the spiciness anomalies by 22 months. This characteristic is evident not only in short-term but also in long-term datasets with very high correlations of 0.92 and 0.72 for MOAA GPV and EN422, respectively.

We further regress the reconstructed spiciness anomalies using CEOF1 with the PDO index at a lag of 22 months (the highest correlation between PDO and the associated PC1) in Fig. 5a. The spatial pattern of CEOF1 associated with the real part is also presented in Fig. 5b. The strongest positive variability in the eastern midlatitude is predominantly explained by the PDO forcing. In addition, there is another region of negative anomaly associated with the PDO forcing, centered at 20° N, 145° W. The defined NPP almost lies in the region of spiciness variability explained by the PDO forcing, thus can be employed to depict the propagation of spiciness anomalies from the source region toward the tropics.

Having established a strong relationship between the PDO and SSAs, it is therefore interesting to see how the spiciness signals evolve following the forcing of PDO. Figure 4b shows the lead-lag correlation between the reconstructed spiciness anomalies using CEOF1 averaged along the NPP and the PDO index. Consistent with the regression in Fig. 5a, the lag correlation exhibits an equatorward

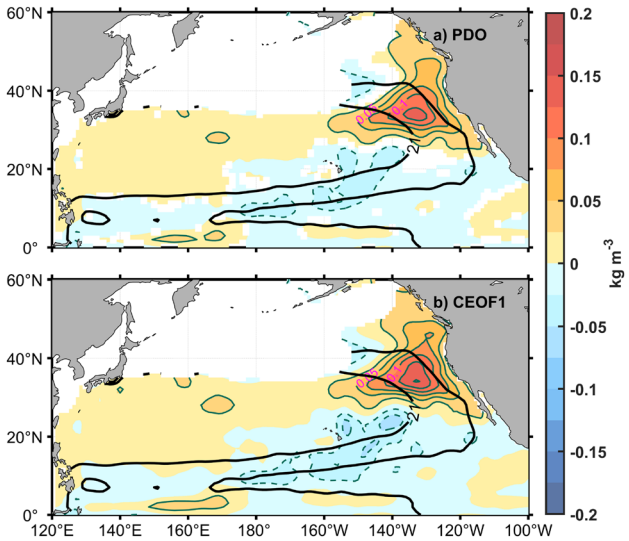

Fig. 5 **a** Reconstructed spiciness anomalies using CEOF1 regressed with the PDO index at lag 22 months (shading and green contours). The contour interval is 0.025 kg m^{-3} and the solid (dashed) contours denote positive (negative) anomalies. **b** Spatial structure of the corresponding CEOF1 (real). The thick black lines represent the defined NPP

evolving positive (negative) pattern that originates from the midlatitude (subtropics). The robustness of the PDO in forcing the subsurface spiciness propagating mode can reach approximately 14° N after 7 years (positive anomaly). The negative anomaly that formed in the eastern subtropics can propagate further equatorward, reaching 10° N after roughly 3 years.

The equatorward subsurface propagation has been hypothesized to modulate the tropical climate variability at decadal time scales (Gu and Philander 1997; Schneider 2000). We further examine the PDO-forced propagating characteristic of the subsurface by regressing the reconstructed spiciness anomalies using CEOF1 with the PDO index from no lag (lag 0) to 7 years later (Fig. 6). A simultaneous dipole pattern of spiciness variability is formed associated with the PDO forcing at no lag: positive in the midlatitude centering at 40° N, 135° W and negative in the subtropics centering at 25° N, 130° W. Afterward, the two anomalous signals propagate equatorward along the NPP. The positive spiciness anomaly not only propagates downstream but also strengthens until 4 years later (lag 48). It then weakens subsequently and continues to propagate until reaching 14° N after 7 years (lag 84). The other negative anomaly formed in the eastern subtropical Pacific can also be observed 3 years later (lag 36) around 10° N with a much stronger magnitude than the above positive anomaly arriving at 14° N. In addition, another negative anomaly (centers at 40° N, 150° W) is formed alternatively in the midlatitude around 2 years later (lag 24). It then gradually amplifies (Stephens et al. 2001) and follows a similar pathway to the positive one to approach the tropics (see also Figs. 2a and S2). This in turn could create a decadal cycle of equatorward ventilation, similar to the hypothesis of Gu and Philander (1997). Further analysis of the power spectrum of the PC1 (real) confirms the robustness of the propagating mode as there is a significant peak within the 8- to 16-year (decadal) periods, similar to the spectral peak of the PDO (Fig. 7a, b).

We also note another robust 6- to 8-year (quasi-decadal) signal, exhibiting a magnitude comparable to the decadal one in both PDO and PC1. This quasi-decadal signal is most pronounced in the subtropical North Pacific (30-40° N, 140-120° W) (Figs. 1a, b and 2) and may effectively propagate to the equatorial region with comparable magnitude retained (Figs. 2a, 4b and 6). We will demonstrate later that the quasi-decadal signal is primarily driven by the Aleutian Low/PDO-induced net surface heat flux and wind stress curl anomalies. Furthermore, the signal becomes more evident after 2000 and may be associated with the recent marine heatwaves in the Northeastern Pacific (Bond et al. 2015). The intricate interplay among the Aleutian Low/PDO, marine heatwaves, and subtropical SSAs warrants further analysis but falls beyond the scope of the present study.

The above analysis has identified the role of PDO in forcing SSAs in both midlatitude and subtropical North Pacific. In addition, the Aleutian Low has been demonstrated as a primary driver of the PDO (Fig. S3). We further investigate the connection between SSAs and the dominant atmospheric forcing of the PDO. Figure 8 shows the regression of SLP, 10-m wind vector, and Qnet (positive downward) anomalies 22 months ahead with the PC1 (real) of spiciness anomalies. As expected, the midlatitude positive spiciness anomalies are associated with the strengthening of the Aleutian Low through the change of PDO (Figs. 5a and 8a). Previous

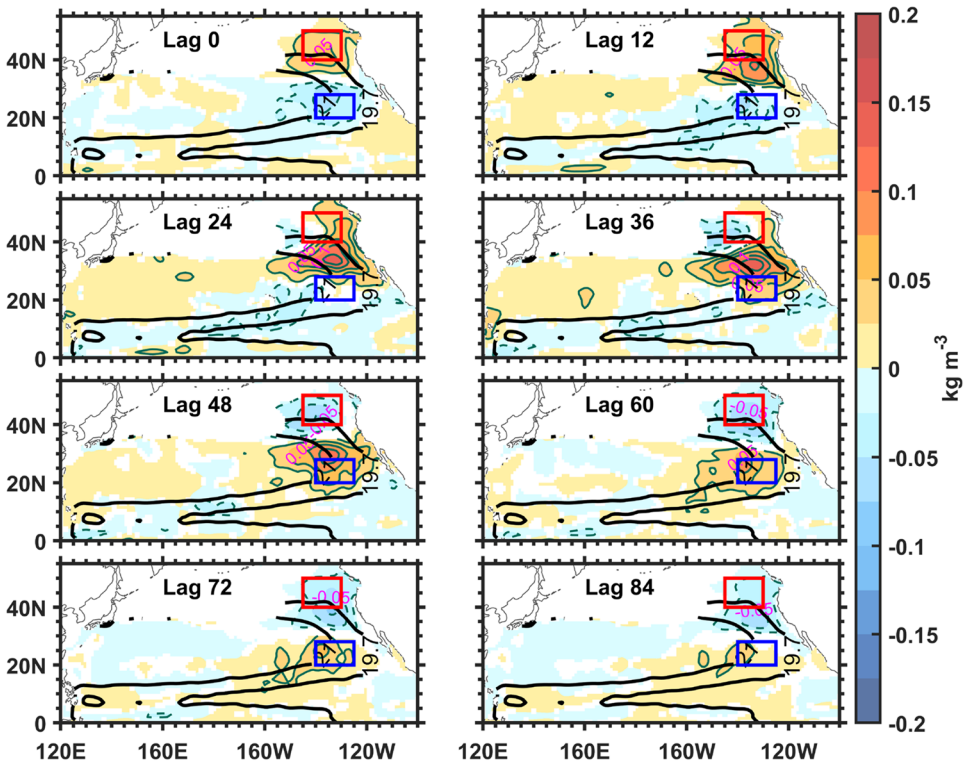

Fig. 6 Reconstructed spiciness anomalies using CEOF1 regressed with the PDO index from lag 0 to lag 84 months (shading and green contours). The contour interval is 0.025 kg m^{-3} and the solid (dashed) contours denote positive (negative) anomalies. The red and blue boxes represent the midlatitude (40–50° N, 145–130° W) and subtropical (20-28° N, 140-125° W) regions, respectively. Thick black lines represent the defined NPP. Positive lags indicate PDO leads the spiciness anomalies

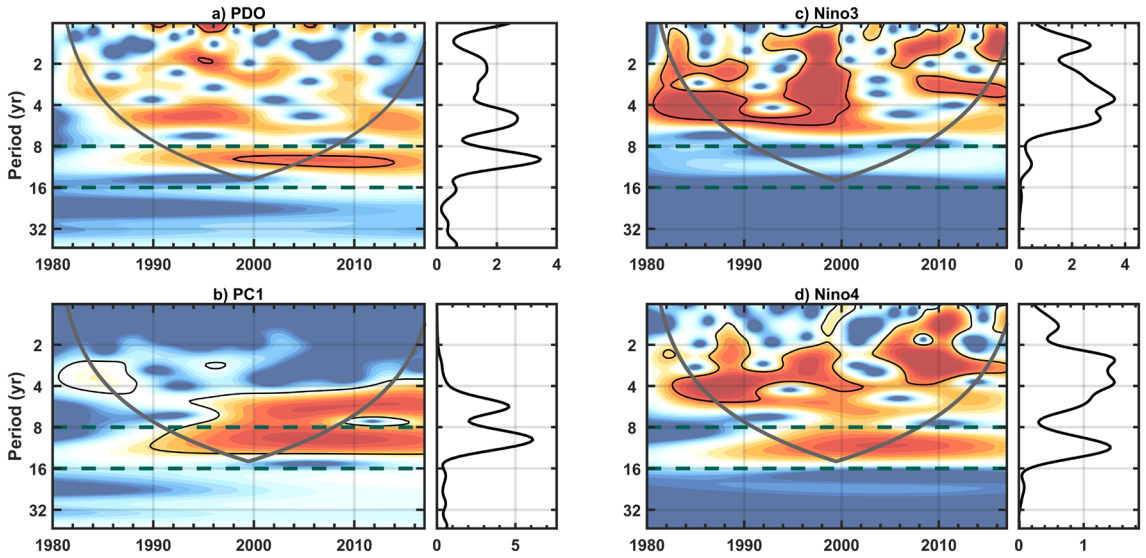

Fig. 7 **a** Bias-rectified wavelet power spectrum and corresponding global wavelet spectrum of PDO from 1980 to 2018. Thin black contours indicate statistically significant at the 95% confidence level when tested against a first-order autoregressive model null hypothesis. The parabola regions indicate the "cone of influence" where edge effects become important. Horizontal dashed green lines indicate the 8- and 16-year periods. **b**–**d** Same as (**a**) but for **b** PC1 (real), **c** Niño3, and **d** Niño4 (5° S-5° N, 160° E–150° W)

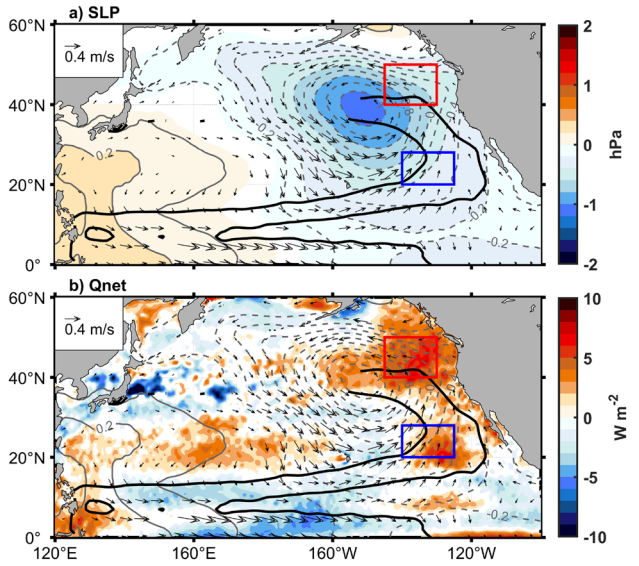

Fig. 8 **a** SLP (hPa, shading and gray contours) and **b** Qnet (W m^{-2}, shading) anomalies regressed with the PC1 of spiciness anomalies (PC1 lags 22 months). 10-m wind vectors regressed with the PC1 are also imposed. The red and blue boxes are described in Fig. 6. Thick black lines represent the defined NPP

studies suggested that the cyclonic wind anomalies associated with the intensified Aleutian Low produce downward heat flux anomalies along the west coast of North America (Yu and Kim 2011), consistent with the band of positive Qnet in the eastern midlatitude in Fig. 8b. This pattern coincides with the positive SSAs in Fig. 5. Therefore, our results confirm that the strengthening of the Aleutian Low drives a positive Qnet anomaly in the eastern midlatitude, forcing the corresponding positive SSAs.

3.3 Formation of isopycnal spiciness anomalies

The generation of SSAs in the eastern extratropical South Pacific has been proposed in terms of both subduction (Nonaka and Sasaki 2007) and spice injection (Yeager and Large 2004; Kolodziejczyk and Gaillard 2012; Wang and Luo 2020). However, the formation of isopycnal spiciness anomalies in the eastern subtropical North Pacific (25–33° N, 150–135° W) can only be ascribed in part to injection during boreal winter (Katsura 2018). In contrast, subduction is proposed for isopycnal temperature variability in the central midlatitude North Pacific (Schneider et al. 1999a). As a result, whether subduction or spice injection can explain the anomalies observed along the isopycnals of 25–26 kg m^{-3} is still unclear.

In Sect. 3.2, we find that the PDO-forced subsurface variability results in a dipole pattern of spiciness anomalies in the midlatitude and subtropics. This suggests that different physical processes are involved in the formation of SSAs. Therefore, we investigate the positive signal in the midlatitude (the red box, Fig. 6) and the negative signal in the subtropics (the blue box, Fig. 6) separately to identify the governing generation mechanisms in the two regions. In general, subsurface spiciness evolution can be determined by the combined vertical variations of temperature and salinity. In addition, surface oceanic conditions favor the formation

of SSAs (Nonaka and Sasaki 2007). By combining these features, we can verify whether subduction or spice injection is relevant to the anomalies along the isopycnals of 25–26 kg m^{-3}.

3.3.1 Midlatitude

Spiciness variability between 25 and 26σ_θ largely follows the pattern of temperature anomalies at around 50–120 m, demonstrating the key role of temperature in regulating SSAs (Fig. 9a, c). Salinity anomalies, however, enhance (weaken) the isopycnal spiciness variability when having the same (opposite) sign with temperature anomalies and are most pronounced below 100 m (Fig. 9b, c). While interior temperature variability can generally be traced to the surface of outcrop, the salinity anomalies between 50 and 120 m are disconnected from surface variability, suggesting different dynamics are involved in the generation of anomalous signals associated with the two variables. Interior salinity variability in this region might relate to the propagation of subsurface salinity anomalies originating in the Gulf of Alaska (Pozo Buil and Di Lorenzo 2015).

To characterize the contribution of subduction versus spice injection in the midlatitude, Fig. 10 shows the maps of the isopycnal $\sigma_\theta = 25$ outcrop position and the standard deviation of March spiciness anomalies averaged between 25 and 26σ_θ. Because the mean isopycnal depth is shallow here

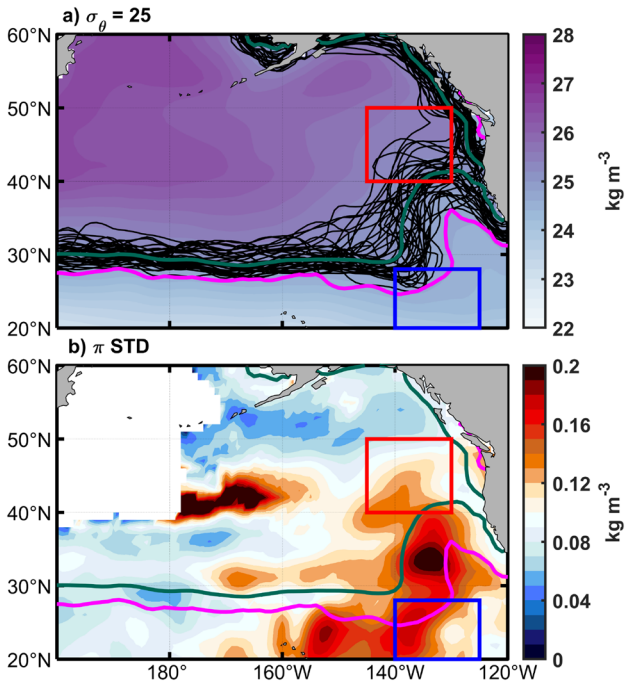

Fig. 10 **a** Annual mean outcrop position of $\sigma_\theta = 25$ surface (thin black contours). The mean March sea surface density (kg m^{-3}) during 1980–2018 is shaded. **b** standard deviation of March spiciness anomalies (kg m^{-3}) averaged between 25 and 26σ_θ. The thick green and magenta contours in both panels denote the mean and extreme equatorward outcrop position of $\sigma_\theta = 25$ in March, respectively. The red and blue boxes are the regions defined in Fig. 6

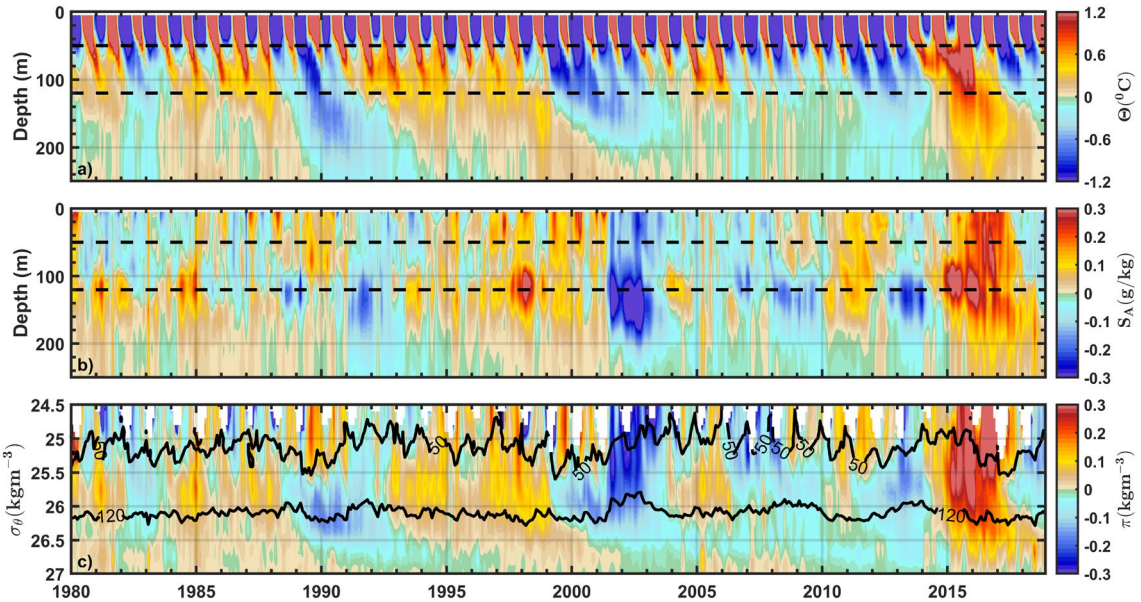

Fig. 9 **a** Time-depth plot of temperature anomalies averaged in 40–50° N, 145–130° W (midlatitude, the red box in Fig. 6) during 1980–2018. The depths of 50 m and 120 m are shown as horizontal dashed black lines. **b** same as (**a**) but for salinity anomalies. **c** Time-σ_θ plot of spiciness anomalies averaged over the same region as **a**. The depths of 50 m and 120 m are shown as the thick black lines

(Fig. S1), $\sigma_\theta = 25$ does expose to the surface and its annual wintertime outcrop position is largely located at the southern edge or even outside the red box (Fig. 10a). In addition, the mean outcrop line is located at the area associated with the large standard deviation of late winter isopycnal spiciness variability while the extreme outcrop line extends further equatorward to the northern edge of the blue box (Fig. 10b). Therefore, subduction is expected to play a significant role in the formation of SSAs in the midlatitude.

Figure 11 further shows the temporal evolution of the isopycnal $\sigma_\theta = 25$ outcrop latitude, spiciness anomalies averaged between $\sigma_\theta = 25$–26, SSTA and SSS anomalies in March. The $\sigma_\theta = 25$ displaces meridionally from its mean position of 35.5° N which is largely explained by the variation of SSTA associated with PDO (the correlation between SSTA and PDO is 0.75, $p < 0.01$). The temporal evolution of isopycnal spiciness anomalies almost tracks the variability of SSTA, but some out-of-phase variations do occur. This suggests that a variety of surface forcing might play different roles in the formation of SSAs. To examine how subduction generates SSAs, two representative years are selected for example, in 2015 when the sea surface was warm and the outcrop line migrated poleward, and in 2017 when the sea surface was cold and the outcrop line migrated equatorward. The corresponding spatial distribution of SSTA, SSS anomalies, and the $\sigma_\theta = 25$ outcrop position is shown in Fig. 12. In 2015, surface oceanic variability around the red box was characterized by strong positive SSTA and relatively weak SSS anomalies (Fig. 12a, c). The warm SSTA caused the isopycnal σ_θ =25 to migrate poleward from its mean position, forming the positive spiciness anomalies (Fig. 11a). In this case of "purely" subduction, isopycnal spiciness anomalies have the same sign as SSTA. In 2017, the anomalously cold SSTA caused the isopycnal $\sigma_\theta = 25$ to migrate equatorward from its mean position. Supposedly, negative SSAs were expected but positive signals were found (Fig. 11a). This is because the strong positive SSS anomalies have compensated for the impact of negative SSTA to form positive SSAs as demonstrated in Nonaka and Sasaki (2007). In general, when the wintertime PDO-related SSTA dominates over salinity, surface properties subduct into the interior ocean to generate isopycnal spiciness anomalies that mainly exhibit SSTA signature. In contrast, when there is strong meridional compensation between SSTA and SSS anomalies, the resulting isopycnal anomalies vary out of phase with the SSTA.

However, subduction alone cannot fully explain SSAs in the midlatitude North Pacific. The prolonged periods of warm temperature anomalies at around 60–140 m such as during 1991–1995, 1996–1997, 2005–2006, and 2014–2016

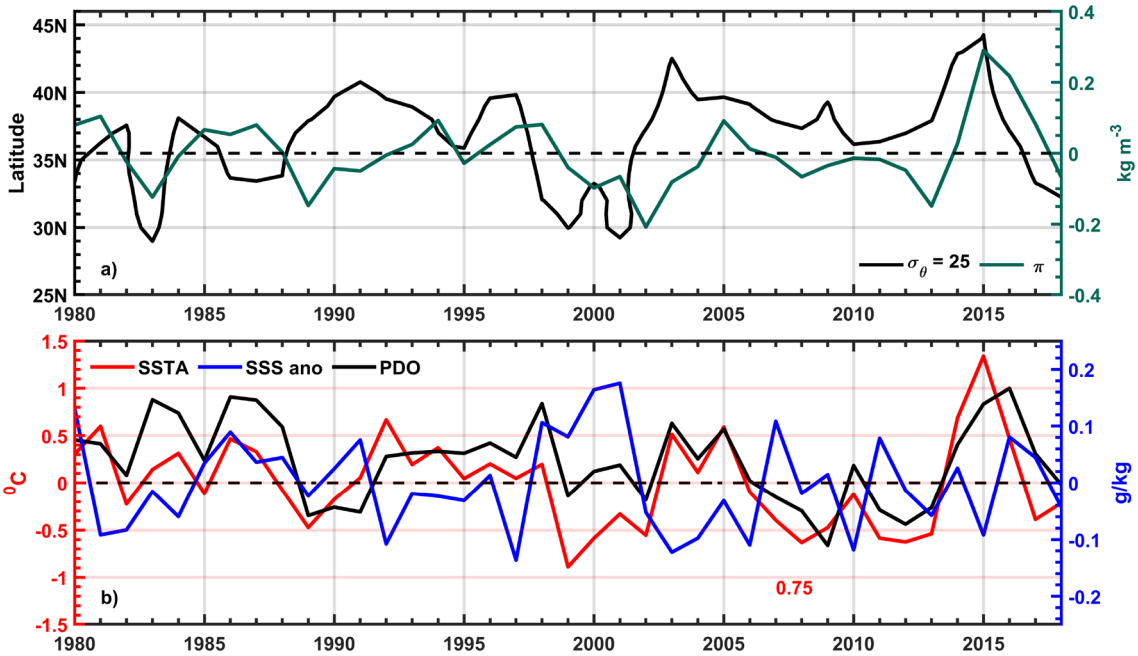

Fig. 11 **a** Time series of March outcrop latitude of $\sigma_\theta = 25$ averaged from 145° to 130° W (black) and the areal mean (the red box) of spiciness anomalies averaged between 25–26σ_θ(green). The mean outcrop latitude of $\sigma_\theta = 25$ is shown by the dashed black line. **b** Time series of the areal mean (35–60° N, 150–115° W) SSTA (red) and SSS anomalies (blue). March PDO index is superimposed (black). The red number is the simultaneous correlation between SSTA and PDO

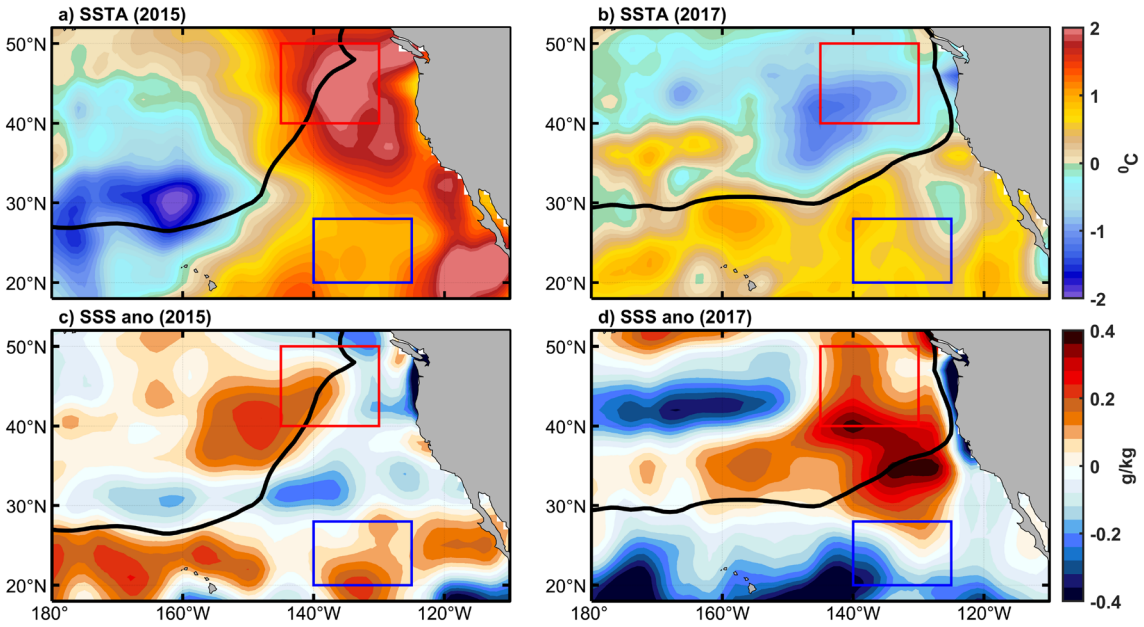

Fig. 12 **a** Monthly mean SSTA (°C) in 2015 March. The corresponding outcrop position of $\sigma_\theta = 25$ is shown as the thick black contours. **b** Sams as **a** but for 2017 March. **c**, **d** Same as (**a**, **b**) but for SSS anomalies (g kg^{-1}). The red and blue boxes are the regions defined in Fig. 6

are associated with the persistence of temperature anomalies via the reemergence mechanism (Alexander and Deser 1995), which reinforces the subsurface signals to the following winter (Fig. S5a) and forms positive spiciness anomalies between 25 and 26σ_θ (Fig. 9a, c). The persistence of negative temperature anomalies in 1999 hindered the downward penetration of positive surface signal in the following winter which in turn induced negative isopycnal spiciness anomalies during 1999–2001. The formation of SSAs in the midlatitude is also consistent with the large reemergence area in the North Pacific (Fig. 1a in Murata et al. (2020)). Therefore, subduction and reemergence are responsible for midlatitude isopycnal spiciness variability.

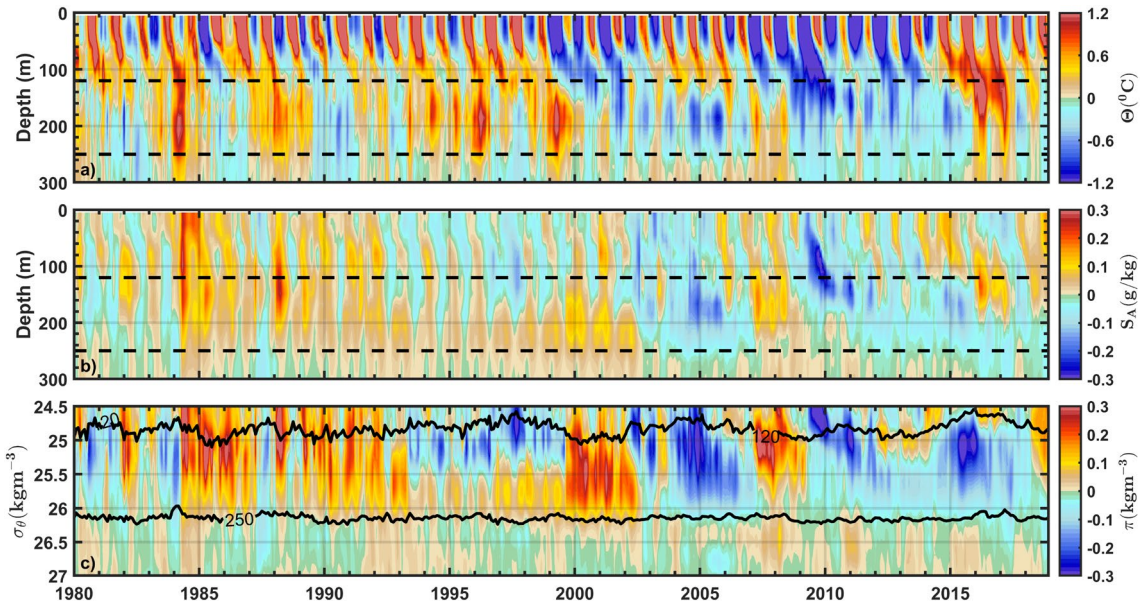

Fig. 13 Same as Fig. 9 but in 20–28° N, 140–125° W (subtropics, the blue box in Fig. 6). The depths of 120 m and 250 m are shown as the horizontal dashed black lines (in **a**, **b**) and the thick black line in (**c**)

3.3.1.1 Subtropics As the isopycnal surface $\sigma_\theta = 25$ outcrops in the northern edge of the blue box (Fig. 10), subduction plays a role in the formation of SSAs in the subtropics. This can be further verified by the persistent penetration of surface temperature anomalies into the interior ocean (Fig. 13a). However, the interannual variability of SSAs in the subtropics greatly follows the variation of salinity anomalies (Fig. 13b, c). For example, the observed positive spiciness anomaly in 1990 between $\sigma_\theta = 25$–26 kg m^{-3} was in tandem with a positive salinity anomaly at around 120–250 m while temperature showed an opposite signature. Due to the critical role of salinity in SSAs (Yeager and Large 2004), spice injection is expected to play a role in the formation of spiciness anomalies in the region. During the winter of 1988, a pulse of greater than normal salinity detrained the interior ocean and thus formed subsurface warm/salty anomalies.

Since spice injection is correlated with the deepening or shallowing of the wintertime mixed layer depth (MLD) (Kolodziejczyk and Gaillard 2013; Wang and Luo 2020), we then determine the terms contributing to MLD changes. Following Wade et al. (2011) and Wang and Luo (2020), we show in Fig. S6a the lead-lag correlation between MLD and Ekman pumping, friction velocity, freshwater flux, and Qnet anomalies. Here the MLD is determined by using 0.2 °C as the temperature threshold following de Boyer Montégut et al. (2004). We find that local MLD changes greatly vary with Qnet and Ekman velocity (Fig. S6a). Both Qnet and Ekman pumping are also closely related to PDO forcing (Fig. S6b). As a result, the Qnet and wind stress curl anomalies associated with the Aleutian low/PDO induce MLD changes to generate SSAs via spice injection (Fig. S6). This result is also consistent with the finding of Katsura (2018).

However, a considerable fraction of salinity variation leading to SSAs is not traceable to the surface, suggesting that processes other than subduction and spice injection are involved in the generation of isopycnal spiciness anomalies. For example, the positive salinity anomaly observed in 1993 was found at a depth below 150 m, completely disconnected from the anomaly above (Fig. 13b). This vertical discontinuity can also be observed during 1996–2002 and 2014–2017. These years coincide with the phase change of the PDO and strong El Niño events (Fig. 3) which can generate anomalous geostrophic currents acting against mean spiciness gradients to form isopycnal spiciness anomalies (Schneider 2000; Kilpatrick et al. 2011). Following Kilpatrick et al. (2011), we regress the SSH anomalies averaged in 36-42° N, 170-155° W (this is the key forcing region for the formation of SSAs via the anomalous advection mechanism as demonstrated in Kilpatrick et al. (2011) and is also coincident with the center of action of the PDO (Fig. S3a). Note that changing the location and size of the forcing region does not change the conclusion drawn here) with the spiciness anomalies averaged between 25 and 26 σ_θ at various time lags. Figure 14 and Fig. S7 suggest that a large fraction of negative signals in the blue box is associated with the wind stress curl anomalies induced SSH variability as shown in Kilpatrick et al. (2011). However, lead-lag correlation analysis between the SSAs averaged in the blue box and the whole North Pacific domain reveals that subtropical SSAs mainly result from the upstream area via the climatological advection of spiciness anomalies rather than locally generated (not shown).

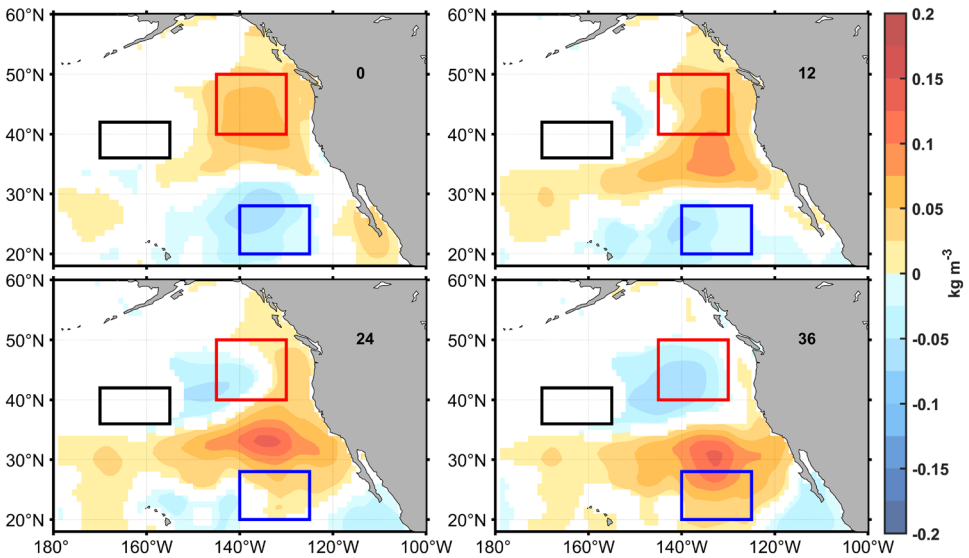

Fig. 14 Spiciness anomalies (kg m^{-3}) averaged between 25 and 26σ_θ regressed with the areal mean (black box) SSH anomalies from lag 0 to lag 36 months (positive indicates SSH leads). The red and blue boxes are the regions defined in Fig. 6

4 Discussion

Generally speaking, the boreal winter atmospheric and surface oceanic forcings lead to the formation of SSAs in the North Pacific. In the eastern midlatitude, the strengthening of the Aleutian Low drives positive Qnet anomalies that induce the corresponding positive SSTA (Figs. S8 and 12). The sea surface density then becomes lower, leading to the poleward migration of the isopycnal surface $\sigma_\theta = 25$ (Figs. 11 and 12). Depending upon the degree of meridional compensation between SSTA and SSS anomalies (Nonaka and Sasaki 2007), the resulting isopycnal spiciness anomalies can have the same or opposite sign with the SSTA (Fig. 11). In addition, the winter-to-winter persistence of subsurface temperature signals also contributes to the formation of SSAs via the reemergence mechanism (Fig. S5). In the eastern subtropics, both subduction and spice injection contribute to isopycnal spiciness anomalies (Figs. 10 and 13). The latter is associated with the deepening or shoaling of the MLD due to the Aleutian Low/PDO-induced Qnet and wind stress curl anomalies (Fig. S6). Furthermore, the variability of the flow pattern as a result of the interaction between the Aleutian Low and PDO generates isopycnal spiciness anomalies in the extratropical region (Fig. 14).

Spiciness is useful to track the water mass variation which can relate to low-frequency ocean climate variability. For the observed SSA change of magnitude ± 0.03 kg m^{-3} at 10° N (Fig. 2a), the corresponding temperature and salinity anomalies can reach more than ± 0.1 °C and ± 0.02 g/kg, respectively (not shown). Thus, the emergence of extratropical origin of spiciness anomalies in the central-eastern equatorial Pacific is of great interest because of their key role in driving tropical climate variability (Gu and Philander 1997; Schneider 2000; Zeller et al. 2021). By artificially imposing continual interior perturbations in the western equatorial Pacific, Schneider (2004) showed that the arrival of spiciness signals can induce a modest coupled mode of ocean–atmosphere response in the tropics. The occurrences of subsurface warming during 2003–2005 and cooling during 2008–2010 in the central equatorial Pacific were hypothesized to initiate the weak 2004–2005 El Niño and strong 2010–2011 La Niña events (Li et al. 2012). However, in the present study, the impact of extratropical spiciness anomalies on tropical climate variability is still unclear due to the short record of the dataset employed.

Moreover, the emergence of subsurface signals in the off-equatorial Pacific, resulting from the SSAs through the NPP, has been hypothesized to act as an oceanic "precursor" triggering the onset of El Niño-Southern Oscillation (ENSO) (Ding et al. 2015). When these low-frequency signals reach the subtropical and tropical boundary, the subtropical-tropical cell (STC) (Liu 1994; McCreary and Lu 1994; Capotondi et al. 2005) and tropical dynamics start to play a role (Chen et al. 2015). In Fig. 2, consistent warm anomalies were observed equatorward of 10° N that precede those strong and very strong El Niño events for about one year, serving as a pre-conditioned heat content for the ENSO variability. These positive anomalies in conjunction with the impact of the Victoria mode, defined as the second EOF of SSTA poleward of 20° N, may further initiate an anomalous signal of similar sign in the central-eastern equatorial Pacific which eventually leads to the development of ENSO (Ding et al. 2015).

Our study confirms the evolution of SSAs is forced by extratropical atmospheric forcing, suggesting a potential linkage with (preceding) interannual SST variability in the tropical Pacific through atmospheric teleconnection. Figure 2a reveals that strong El Niño events (decadal signals) are followed by a positive spiciness anomaly, most prominent around 30° N, demonstrating the influence of tropical forcing on the formation of the subsurface spiciness mode. Indeed, the highest correlations of PC1 (real) with Niño3 and Niño4 SST indices are 0.48 (PC1 lags 22 months) and 0.61 (PC1 lags 28 months), respectively (Fig. 15a) (Note that the Niño4 SST index appears to lead the PDO by 6 months. This is mainly because the central Pacific ENSO leads the Aleutian Low by 3 months (Yu and Kim 2011) while the Aleutian Low also leads the PDO by 3 months (Fig. S3). Consequently, there is a lead-lag timescale of approximately 6 months between changes in the Niño4 SST anomalies and the PDO). The regression maps of reconstructed spiciness anomalies using CEOF1 with the Niño3 (at lag 22 months) and Niño4 (at lag 28 months) SST indices account for a large fraction of the positive and negative subsurface signals in the midlatitude and subtropics, respectively (Fig. S9), similar to the pattern associated with PDO forcing (Fig. 5a). The main difference between the PDO and tropical forcing is the negative anomaly center at 40° N, 150° W that can only be explained by the former, confirming the primary role of extratropical air-sea interaction in driving the spiciness mode. This is also supported by the higher correlation between PDO and PC1 at 22 months lead than that between Niño4 SST index at 28 months lead. Additionally, Niño4 has a greater contribution than Niño3 on the formation of SSAs (Figs. 7 and 15), consistent with the twenty-first century shift toward a more Central Pacific (here represented by Niño4) type of ENSO (Lee and McPhaden 2010; McPhaden 2012). We also observe a stronger impact of Niño4 SST variability on the subtropical subsurface spiciness mode than the PDO does (compare Fig. 5a and Fig. S9b), suggesting the role of central tropical forcing in modifying the North Pacific atmospheric circulation pattern to induce the formation of SSAs via anomalous advection and spice injection mechanisms (see Sect. 3.3). In general, the extratropical-tropical

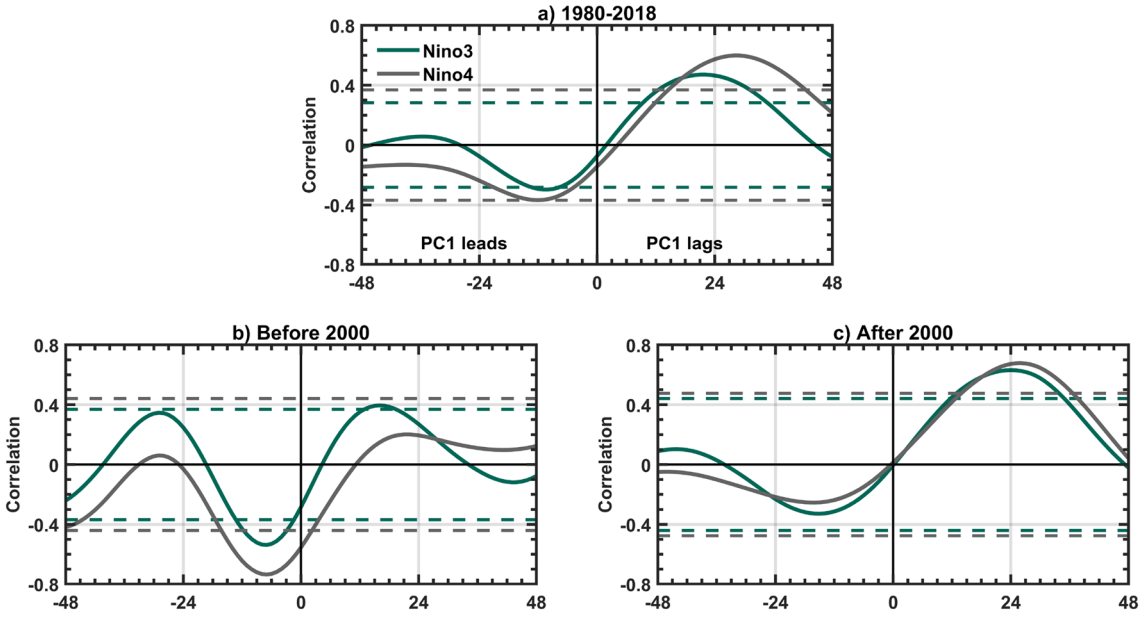

Fig. 15 **a** Lead-lag correlation coefficients between Niño indices and the PC1 of spiciness anomalies (positive indicates Niño indices lead) during 1980–2018. **b**, **c** Same as (**a**) but for the periods before 2000 and after 2000, respectively. Horizontal dashed lines show the 95% confidence level

interaction can potentially generate a decadal climate oscillation in the North Pacific that involves both oceanic and atmospheric bridges.

It is interesting to mention that the SSAs between 25 and 26σ_θ are significantly enhanced within the first few years of their downstream propagation (lags 12–48, Fig. 6). Kilpatrick et al. (2011) suggested that the midlatitude stochastic wind stress curl anomalies can induce local SSH variability, leading to positive and negative SSH anomalies alongshore and offshore, respectively. Our results confirm that the Aleutian low/PDO-related wind stress curl (Fig. S10) and Qnet anomalies (Fig. S8) force the SSH pattern (Fig. S11), which plays a key role in the enhancement of the abovementioned SSAs. The resulting pressure gradient force (pointing from the coastline to offshore) induces subsurface cyclonic circulation, weakening the climatological southward transport, leading to positive spiciness anomalies (Kilpatrick et al. 2011) (Fig. 14). Kilpatrick et al. (2011) also suggested the solely forcing region (black box in Fig. 14) to track the downstream generation of subsurface spiciness signals. Indeed, our results confirm the equatorward amplification of spiciness signals in Fig. 6 is associated with anomalous advection across mean spiciness gradients, consistent with Kilpatrick et al. (2011). Noting that the center of negative SSH anomalies (around 40° N and 160° W, Fig. S11) persists over three consecutive years, resulting from the changes in wind stress curl anomalies (Fig. S10) and Qnet anomalies (Fig. S8) due to the interaction between the Aleutian Low and PDO (Fang and Yang 2016; Luo et al. 2020). Specifically, the meridional SST gradient associated with the mature phase of the PDO (Fig. S3a) can feedback to the overlying atmosphere to strengthen the Aleutian Low (Luo et al. 2020). The strengthened Aleutian Low then further enhances the meridional SST gradient and produces a band of negative and positive Qnet anomalies one year later in the western-central and eastern North Pacific, respectively (Luo et al. 2020) (lag 12, Fig. S8). However, the enhanced meridional SST gradient also generates a band of negative wind stress curl anomalies in the central Pacific (Luo et al. 2020) (lag 12, Fig. S10). These processes lead to the SSH pattern qualitatively similar to those at lag 0. Two years later, the eastern North Pacific is dominated by the alternative sign of wind stress curl anomalies (lag 24, Fig. S10) while weak upward heat flux anomalies are observed in the eastern subtropics (lag 24, Fig. S8), leading to weak negative (positive) SSH anomalies west (east) of 140° W.

Finally, we note that during the boreal winter of 2013–2015, prolonged near-surface warming was observed in the northeastern Pacific, termed the "Pacific warm blob" (Bond et al. 2015) or marine heatwave (Frölicher et al. 2018; Oliver et al. 2018; Smale et al. 2019). The occurrence of this extraordinary phenomenon has been connected with different physical processes, such as the coupling between the North Pacific Gyre Oscillation and PDO due to the two-way tropical-extratropical interactions via atmospheric teleconnection (Di Lorenzo and Mantua 2016; Hu et al. 2017; Joh and Di Lorenzo 2017) and an extended weakening of the North Pacific High (Amaya et al. 2020). The "warm blob"

overlies the region of interior spiciness formation in the midlatitude (Fig. 6). In 2013, a positive surface temperature anomaly can penetrate as deep as 200 m (Hu et al. 2017) and precedes the positive surface salinity anomaly for around half a year (Fig. 9a, b). However, variations of salinity and temperature are almost in phase below 80 m depth and these subsurface signals persist year-round until 2017. As a result, the strongest warm/salty anomaly is produced in the interior ocean (Fig. 9c). Given the strong connection between the warm blob and PDO (Joh and Di Lorenzo 2017) and future projections of the intensification of extreme Aleutian Low events (Giamalaki et al. 2021) as well as the increasing variance of PDO under greenhouse forcing (Di Lorenzo and Mantua 2016), the longer and more frequent occurrence of marine heatwaves (Frölicher et al. 2018; Oliver et al. 2018) could lead to greater subsurface spiciness variability and have a stronger impact on Pacific climate variability (Tseng et al. 2017).

5 Conclusions

This study demonstrates that the Aleutian Low/PDO can induce a dipole pattern of positive and negative SSAs in the midlatitude and subtropics, respectively. The conceptual representation of this spiciness mode is shown in Fig. 16. Specifically, the wintertime intensified Aleutian Low (with contributions from ENSO) induces positive SSTA (PDO positive phase) primarily via Qnet changes in the midlatitude. The resulting sea surface density migrates poleward, allowing surface properties to follow outcrop isopycnals into the interior ocean (subduction mechanism), thereby generating isopycnal spiciness anomalies. The reemergence also contributes to the formation of SSAs, resulting in midlatitude isopycnal spiciness variability that largely aligns with temperature anomaly patterns at around 50–120 m depth. Conversely, the formation of subtropical SSAs is attributed to a combination of local and remote processes. The local process involves subduction and spice injection, wherein the latter is driven by changes in MLD induced by anomalous Qnet and Ekman pumping associated with the Aleutian Low/PDO. The remote process, on the other hand, encompasses the mean advection of spiciness signals from upstream areas. The interplay between these two processes gives rise to isopycnal spiciness anomalies that generally correspond to the variability of salinity anomalies at around 120–250 m depth. Furthermore, the coupling between the Aleutian Low and PDO leads to a persistent year-to-year pattern of SSH anomalies with opposite signs alongshore and offshore. This particular pattern facilitates the strengthening of spiciness signals from the midlatitude to the subtropics through anomalous advection across mean spiciness gradients. The reverse process applies to the opposite phase of the Aleutian Low/PDO.

The study also shows that the resulting dipole pattern of spiciness anomalies can propagate equatorward along the defined NPP. The positive anomaly of midlatitude origin can reach 14° N after 7 years of propagation while the negative anomaly of subtropical origin can arrive at 10° N after 3 years. In addition, a negative anomaly emerges in the midlatitude after the occurrence of the positive signal 2 years later, then follows the pathway that the positive takes to reach the tropics. This ultimately leads to a decadal propagating mode of SSAs in the North Pacific. Although the present study reveals that the decadal spiciness mode can propagate toward the tropical region, the impact of these

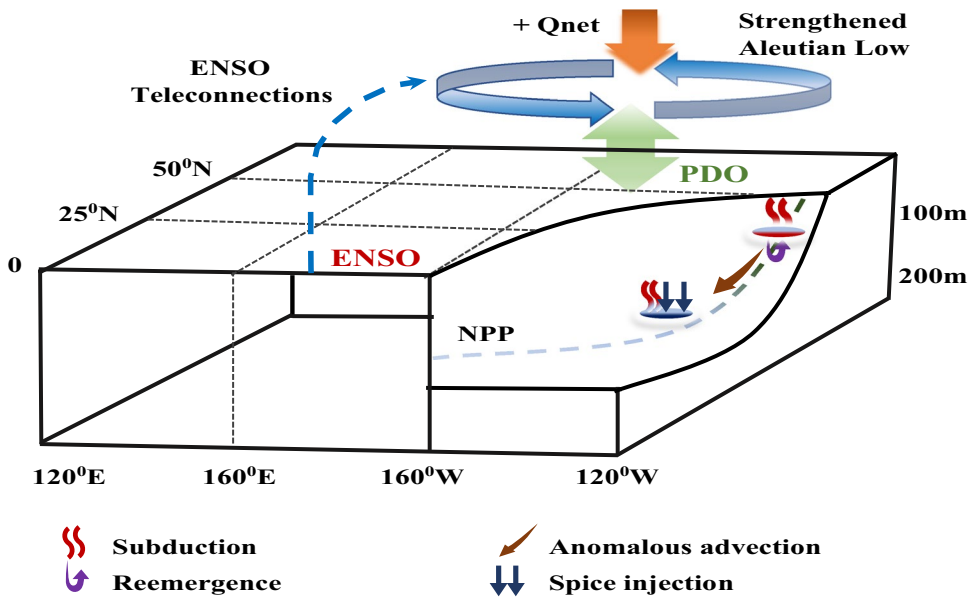

Fig. 16 Schematic of decadal spiciness mode in the North Pacific. The solid red (dark blue) oval indicates positive (negative) spiciness anomalies in the midlatitude (subtropics)

spiciness anomalies on equatorial SST variability at interannual to decadal timescales still requires further investigation.

Supplementary Information The online version contains supplementary material available at https://doi.org/10.1007/s00382-023-06938-w.

Funding The authors express their gratitude to the editor and two anonymous reviewers for valuable comments and suggestions. Computer time was made available by National Center for High-performance Computing (NCHC) of National Applied Research Laboratories (NARLabs) in Taiwan. This research was supported by the NSTC Grant 111-2111-M-002-015 and 112-2611-M-002-016-MY3, Taiwan.

Data availability The TEOS-10 is available at https://www.teos-10.org/software.htm. The CEOF routine can be obtained from http://hydr.ct.tudelft.nl/wbk/public/hooimeijer. Links to data sets used in the paper: EN422: https://www.metoffice.gov.uk/hadobs/en4/download-en4-2-2.html, MOAA GPV: https://www.jamstec.go.jp/argo_research/dataset/moaagpv/moaa_en.html, ERA5: https://www.ecmwf.int/en/forecasts/datasets/reanalysis-datasets/era5, GODAS: https://psl.noaa.gov/data/gridded/data.godas.html.

Declarations

Conflict of interest The authors declare that there are no conflicts of interest or competing interests regarding the publication of this paper.

References

Alexander MA (1990) Simulation of the response of the North Pacific ocean to the anomalous atmospheric circulation associated with El Niño. Clim Dyn 5:53–65. https://doi.org/10.1007/BF00195853

Alexander MA (1992) Midlatitude atmosphere-ocean interaction during El Niño. Part I: the North Pacific ocean. J Clim 5:944–958. https://doi.org/10.1175/1520-0442(1992)005%3c0959:MAIDEN%3e2.0.CO;2

Alexander MA, Deser C (1995) A mechanism for the recurrence of wintertime midlatitude SST anomalies. J Phys Oceanogr 25:122–137. https://doi.org/10.1175/1520-0485(1995)025%3c0122:Amftro%3e2.0.Co;2

Alexander MA, Vimont DJ, Chang P, Scott JD (2010) The impact of extratropical atmospheric variability on ENSO: Testing the seasonal footprinting mechanism using coupled model experiments. J Clim 23:2885–2901. https://doi.org/10.1175/2010JCLI3205.1

Amaya DJ, Miller AJ, Xie S-P, Kosaka Y (2020) Physical drivers of the summer 2019 North Pacific marine heatwave. Nat Commun 11:1903. https://doi.org/10.1038/s41467-020-15820-w

Barnett TP (1983) Interaction of the monsoon and Pacific trade wind system at interannual time scales Part I: the equatorial zone. Mon Weather Rev 111:756–773. https://doi.org/10.1175/1520-0493(1983)111%3c0756:IOTMAP%3e2.0.CO;2

Behringer DW, Xue Y (2004) Evaluation of the global ocean data assimilation system at NCEP: The Pacific Ocean. In: Eighth symposium on integrated observing and assimilation systems for atmosphere, oceans, and land surface, AMS 84th annual meeting, Washington State Convention and Trade Center, Seattle, Washington, pp 11–15. https://ams.confex.com/ams/84Annual/techprogram/paper_70720.htm

Behringer DW, Ji M, Leetmaa A (1998) An improved coupled model for ENSO prediction and implications for ocean initialization. Part I: The ocean data assimilation system. Mon Weather Rev 126:1013–1021. https://doi.org/10.1175/1520-0493(1998)126%3c1013:AICMFE%3e2.0.CO;2

Bond NA, Cronin MF, Freeland H, Mantua N (2015) Causes and impacts of the 2014 warm anomaly in the NE Pacific. Geophys Res Lett 42:3414–3420. https://doi.org/10.1002/2015GL063306

Byrne MP, Pendergrass AG, Rapp AD, Wodzicki KR (2018) Response of the intertropical convergence zone to climate change: Location, width, and strength. Curr Clim Change Rep 4:355–370. https://doi.org/10.1007/s40641-018-0110-5

Capotondi A, Alexander MA, Deser C, McPhaden MJ (2005) Anatomy and decadal evolution of the Pacific Subtropical-Tropical Cells (STCs). J Clim 18:3739–3758. https://doi.org/10.1175/jcli3496.1

Chen H-C, Sui C-H, Tseng Y-H, Huang B (2015) An analysis of the linkage of Pacific subtropical cells with the recharge-discharge processes in ENSO evolution. J Clim 28:3786–3805. https://doi.org/10.1175/jcli-d-14-00134.1

Davis RE (1977) Techniques for statistical analysis and prediction of geophysical fluid systems. Geophys Astrophys Fluid Dyn 8:245–277. https://doi.org/10.1080/03091927708240383

de Boyer Montégut C, Madec G, Fischer AS, Lazar A, Iudicone D (2004) Mixed layer depth over the global ocean: an examination of profile data and a profile-based climatology. J Geophys Res Oceans. https://doi.org/10.1029/2004JC002378

Di Lorenzo E, Mantua N (2016) Multi-year persistence of the 2014/15 North Pacific marine heatwave. Nat Clim Change 6:1042–1047. https://doi.org/10.1038/nclimate3082

Ding R, Li J, Tseng Y-h, Sun C, Guo Y (2015) The Victoria mode in the North Pacific linking extratropical sea level pressure variations to ENSO. J Geophys Res Atmos 120:27–45. https://doi.org/10.1002/2014JD022221

Fang J, Yang X-Q (2016) Structure and dynamics of decadal anomalies in the wintertime midlatitude North Pacific ocean–atmosphere system. Clim Dyn 47:1989–2007. https://doi.org/10.1007/s00382-015-2946-x

Flament P (2002) A state variable for characterizing water masses and their diffusive stability: spiciness. Prog Oceanogr 54:493–501. https://doi.org/10.1016/S0079-6611(02)00065-4

Frölicher TL, Fischer EM, Gruber N (2018) Marine heatwaves under global warming. Nature 560:360–364. https://doi.org/10.1038/s41586-018-0383-9

Fukumori I, Lee T, Cheng B, Menemenlis D (2004) The origin, pathway, and destination of Niño-3 water estimated by a simulated passive tracer and its adjoint. J Phys Oceanogr 34:582–604. https://doi.org/10.1175/2515.1

Giamalaki K, Beaulieu C, Henson SA, Martin AP, Kassem H, Faranda D (2021) Future intensification of extreme Aleutian low events and their climate impacts. Sci Rep 11:18395. https://doi.org/10.1038/s41598-021-97615-7

Giese BS, Urizar SC, Fučkar NS (2002) Southern Hemisphere origins of the 1976 climate shift. Geophys Res Lett 29:1-1–1-4. https://doi.org/10.1029/2001GL013268

Good SA, Martin MJ, Rayner NA (2013) EN4: Quality controlled ocean temperature and salinity profiles and monthly objective analyses with uncertainty estimates. J Geophys Res Oceans 118:6704–6716. https://doi.org/10.1002/2013JC009067

Gu D, Philander SGH (1997) Interdecadal climate fluctuations that depend on exchanges between the tropics and extratropics. Science 275:805–807. https://doi.org/10.1126/science.275.5301.805

Hasselmann K (1976) Stochastic climate models Part I. Theory. Tellus 28:473–485. https://doi.org/10.3402/tellusa.v28i6.11316

Hazeleger W, Visbeck M, Cane M, Karspeck A, Naik N (2001) Decadal upper ocean temperature variability in the tropical Pacific. J Geophys Res Oceans 106:8971–8988. https://doi.org/10.1029/2000JC000536

Hersbach H et al (2020) The ERA5 global reanalysis. Q J R Meteorol Soc 146:1999–2049. https://doi.org/10.1002/qj.3803
Horel JD (1984) Complex principal component analysis: theory and examples. J Appl Meteorol Climatol 23:1660–1673. https://doi.org/10.1175/1520-0450(1984)023%3c1660:CPCATA%3e2.0.CO;2
Hosoda S, Ohira T, Nakamura T (2008) A monthly mean dataset of global oceanic temperature and salinity derived from Argo float observations. JAMSTEC Rep Res Dev 8:47–59. https://doi.org/10.5918/jamstecr.8.47
Hu Z-Z, Kumar A, Jha B, Zhu J, Huang B (2017) Persistence and predictions of the remarkable warm anomaly in the northeastern Pacific ocean during 2014–16. J Clim 30:689–702. https://doi.org/10.1175/jcli-d-16-0348.1
Huang RX (2011) Defining the spicity. J Mar Res 69:545–559. https://doi.org/10.1357/002224011799849390
Huang RX, Yu LS, Zhou SQ (2018) New definition of potential spicity by the least square method. J Geophys Res Oceans 123:7351–7365. https://doi.org/10.1029/2018jc014306
Huang RX, Yu LS, Zhou SQ (2021) Quantifying climate signals: Spicity, orthogonality, and distance. J Geophys Res Oceans. https://doi.org/10.1029/2020JC016646
Jackett DR, Mcdougall TJ (1985) An oceanographic variable for the characterization of intrusions and water masses. Deep Sea ResPart A Oceanogr Res Papers 32:1195–1207. https://doi.org/10.1016/0198-0149(85)90003-2
Joh Y, Di Lorenzo E (2017) Increasing coupling between NPGO and PDO leads to prolonged marine heatwaves in the northeast Pacific. Geophys Res Lett 44:11663–611671. https://doi.org/10.1002/2017GL075930
Katsura S (2018) Properties, formation, and dissipation of the North Pacific eastern subtropical mode water and its impact on interannual spiciness anomalies. Prog Oceanogr 162:120–131. https://doi.org/10.1016/j.pocean.2018.02.023
Kilpatrick T, Schneider N, Di Lorenzo E (2011) Generation of low-frequency spiciness variability in the thermocline. J Phys Oceanogr 41:365–377. https://doi.org/10.1175/2010jpo4443.1
Kolodziejczyk N, Gaillard F (2012) Observation of spiciness interannual variability in the Pacific pycnocline. J Geophys Res Oceans. https://doi.org/10.1029/2012JC008365
Kolodziejczyk N, Gaillard F (2013) Variability of the heat and salt budget in the subtropical southeastern Pacific mixed layer between 2004 and 2010: Spice injection mechanism. J Phys Oceanogr 43:1880–1898. https://doi.org/10.1175/JPO-D-13-04.1
Lee T, McPhaden MJ (2010) Increasing intensity of El Niño in the central-equatorial Pacific. Geophys Res Lett. https://doi.org/10.1029/2010GL044007
Li YL, Wang F, Sun Y (2012) Low-frequency spiciness variations in the tropical Pacific ocean observed during 2003–2012. Geophys Res Lett. https://doi.org/10.1029/2012GL053971
Liu Z (1994) A simple model of the mass exchange between the subtropical and tropical ocean. J Phys Oceanogr 24:1153–1165. https://doi.org/10.1175/1520-0485(1994)024%3c1153:Asmotm%3e2.0.Co;2
Liu Z (2012) Dynamics of interdecadal climate variability: a historical perspective. J Clim 25:1963–1995. https://doi.org/10.1175/2011JCLI3980.1
Liu Z, Shin S-I (1999) On thermocline ventilation of active and passive tracers. Geophys Res Lett 26:357–360. https://doi.org/10.1029/1998GL900315
Lu P, McCreary JP (1995) Influence of the ITCZ on the flow of thermocline water from the subtropical to the equatorial Pacific ocean. J Phys Oceanogr 25:3076–3088. https://doi.org/10.1175/1520-0485(1995)025%3c3076:Iotiot%3e2.0.Co;2
Luo JJ, Rothstein LM, Zhang RH, Busalacchi AJ (2005) On the connection between South Pacific subtropical spiciness anomalies and decadal equatorial variability in an ocean general circulation model. J Geophys Res Oceans. https://doi.org/10.1029/2004JC002655
Luo H, Zheng F, Keenlyside N, Zhu J (2020) Ocean-atmosphere coupled Pacific decadal variability simulated by a climate model. Clim Dyn 54:4759–4773. https://doi.org/10.1007/s00382-020-05248-9
Lyon B, Barnston AG, DeWitt DG (2014) Tropical Pacific forcing of a 1998–1999 climate shift: observational analysis and climate model results for the boreal spring season. Clim Dyn 43:893–909. https://doi.org/10.1007/s00382-013-1891-9
Mantua NJ, Hare SR, Zhang Y, Wallace JM, Francis RC (1997) A Pacific interdecadal climate oscillation with impacts on salmon production. Bull Am Meteorol Soc 78:1069–1080. https://doi.org/10.1175/1520-0477(1997)078%3c1069:Apicow%3e2.0.Co;2
McCreary JP, Lu P (1994) Interaction between the subtropical and equatorial ocean circulations: the subtropical cell. J Phys Oceanogr 24:466–497. https://doi.org/10.1175/1520-0485(1994)024%3c0466:Ibtsae%3e2.0.Co;2
McDougall TJ, Barker PM (2011) Getting started with TEOS-10 and the Gibbs Seawater (GSW) oceanographic toolbox. Scor/iapso WG 127:1–28
McDougall TJ, Klocker A (2010) An approximate geostrophic streamfunction for use in density surfaces. Ocean Model 32:105–117. https://doi.org/10.1016/j.ocemod.2009.10.006
McDougall TJ, Krzysik OA (2015) Spiciness. J Mar Res 73:141–152. https://doi.org/10.1357/002224015816665589
McDougall TJ, Barker PM, Stanley GJ (2021) Spice variables and their use in physical oceanography. J Geophys Res Oceans 126:e2019JC015936. https://doi.org/10.1029/2019JC015936
McPhaden MJ (2012) A 21st century shift in the relationship between ENSO SST and warm water volume anomalies. Geophys Res Lett. https://doi.org/10.1029/2012GL051826
Müller P, Willebrand J (1986) Compressibility effects in the thermohaline circulation: a manifestation of the temperature-salinity mode. Deep Sea Res Part A Oceanogr Res Papers 33:559–571. https://doi.org/10.1016/0198-0149(86)90053-1
Munk W (1981) Internal waves and small-scale processes. In: Evolution of physical oceanography, chap 9. MIT Press, Cambridge, Massachusetts, pp 264–291
Murata K, Kido S, Tozuka T (2020) Role of reemergence in the central North Pacific revealed by a mixed layer heat budget analysis. Geophys Res Let 47:e2020GL08194. https://doi.org/10.1029/2020GL088194
Newman M, Compo GP, Alexander MA (2003) ENSO-forced variability of the Pacific Decadal Oscillation. J Clim 16:3853–3857. https://doi.org/10.1175/1520-0442(2003)016%3c3853:EVOTPD%3e2.0.CO;2
Newman M et al (2016) The Pacific decadal oscillation, revisited. J Clim 29:4399–4427. https://doi.org/10.1175/JCLI-D-15-0508.1
Nonaka M, Sasaki H (2007) Formation mechanism for isopycnal temperature-salinity anomalies propagating from the eastern South Pacific to the equatorial region. J Clim 20:1305–1315. https://doi.org/10.1175/Jcli4065.1
Oliver ECJ et al (2018) Longer and more frequent marine heatwaves over the past century. Nat Commun 9:1324. https://doi.org/10.1038/s41467-018-03732-9
Pierce DW (2001) Distinguishing coupled ocean–atmosphere interactions from background noise in the North Pacific. Prog Oceanogr 49:331–352. https://doi.org/10.1016/S0079-6611(01)00029-5
Pierce DW, Barnett TP, Latif M (2000) Connections between the Pacific ocean tropics and midlatitudes on decadal timescales. J

Clim 13:1173–1194. https://doi.org/10.1175/1520-0442(2000)013%3c1173:Cbtpot%3e2.0.Co;2
Pozo Buil M, Di Lorenzo E (2015) Decadal changes in Gulf of Alaska upwelling source waters. Geophys Res Lett 42:1488–1495. https://doi.org/10.1002/2015GL063191
Sasaki YN, Schneider N, Maximenko N, Lebedev K (2010) Observational evidence for propagation of decadal spiciness anomalies in the North Pacific. Geophys Res Lett. https://doi.org/10.1029/2010GL042716
Schneider N (2000) A decadal spiciness mode in the tropics. Geophys Res Lett 27:257–260. https://doi.org/10.1029/1999gl002348
Schneider N (2004) The response of tropical climate to the equatorial emergence of spiciness anomalies. J Clim 17:1083–1095. https://doi.org/10.1175/1520-0442(2004)017%3c1083:Trotct%3e2.0.Co;2
Schneider N, Cornuelle BD (2005) The forcing of the Pacific Decadal Oscillation. J Clim 18:4355–4373. https://doi.org/10.1175/jcli3527.1
Schneider N, Miller AJ, Alexander MA, Deser C (1999a) Subduction of decadal North Pacific temperature anomalies: Observations and dynamics. J Phys Oceanogr 29:1056–1070. https://doi.org/10.1175/1520-0485(1999)029%3c1056:Sodnpt%3e2.0.Co;2
Schneider N, Venzke S, Miller AJ, Pierce DW, Barnett TP, Deser C, Latif M (1999b) Pacific thermocline bridge revisited. Geophys Res Lett 26:1329–1332. https://doi.org/10.1029/1999GL900222
Smale DA et al (2019) Marine heatwaves threaten global biodiversity and the provision of ecosystem services. Nat Clim Chang 9:306–312. https://doi.org/10.1038/s41558-019-0412-1
Stephens M, Liu Z, Yang H (2001) Evolution of subduction planetary waves with application to North Pacific decadal thermocline variability. J Phys Oceanogr 31:1733–1746. https://doi.org/10.1175/1520-0485(2001)031%3c1733:Eospww%3e2.0.Co;2
Stommel H (1962) On the cause of the temperature-salinity curve in the ocean. Proc Natl Acad Sci 48:764–766. https://doi.org/10.1073/pnas.48.5.764
Tailleux R (2016) Generalized patched potential density and thermodynamic neutral density: two new physically based quasi-neutral density variables for ocean water masses analyses and circulation studies. J Phys Oceanogr 46:3571–3584. https://doi.org/10.1175/JPO-D-16-0072.1
Tailleux R (2021) Spiciness theory revisited, with new views on neutral density, orthogonality, and passiveness. Ocean Sci 17:203–219. https://doi.org/10.5194/os-17-203-2021
Tseng Y-H, Ding R, Huang X-m (2017) The warm blob in the northeast Pacific-the bridge leading to the 2015/16 El Niño. Environ Res Lett 12:054019. https://doi.org/10.1088/1748-9326/aa67c3
Veronis G (1972) On properties of seawater defined by temperature, salinity, and pressure. J Mar Res 30:227–255
Wade M, Caniaux G, du Penhoat Y (2011) Variability of the mixed layer heat budget in the eastern equatorial Atlantic during 2005–2007 as inferred using Argo floats. J Geophys Res Oceans. https://doi.org/10.1029/2010JC006683
Wang YY, Luo YY (2020) Variability of spice injection in the upper ocean of the southeastern Pacific during 1992–2016. Clim Dyn 54:3185–3200. https://doi.org/10.1007/s00382-020-05164-y
Yeager SG, Large WG (2004) Late-winter generation of spiciness on subducted isopycnals. J Phys Oceanogr 34:1528–1547. https://doi.org/10.1175/1520-0485(2004)034%3c1528:LGOSOS%3e2.0.CO;2
Yu J-Y, Kim ST (2011) Relationships between extratropical sea level pressure variations and the central Pacific and eastern Pacific types of ENSO. J Clim 24:708–720. https://doi.org/10.1175/2010jcli3688.1
Zeller M, McGregor S, van Sebille E, Capotondi A, Spence P (2021) Subtropical-tropical pathways of spiciness anomalies and their impact on equatorial Pacific temperature. Clim Dyn 56:1131–1144. https://doi.org/10.1007/s00382-020-05524-8
Zhang R-H, Liu Z (1999) Decadal thermocline variability in the North Pacific ocean: two pathways around the subtropical gyre. J Clim 12:3273–3296. https://doi.org/10.1175/1520-0442(1999)012%3c3273:DTVITN%3e2.0.CO;2